THESIS

NMR THERMOMETRY OF VANADIUM BASED LIGAND-TO-METAL-CHARGE-TRANSFER COMPLEXES

Submitted by

Josef Grundy

Department of Chemistry

In partial fulfillment of the requirements

For the Degree of Master of Science

Colorado State University

Fort Collins, Colorado

Summer 2023

Master's Committee:

Advisor: Joe Zadrozny
Co-Advisor: Debbie Crans

Mingzhong Wu

ABSTRACT

NMR THERMOMETRY OF VANADIUM BASED LIGAND-TO-METAL-CHARGE-TRANSFER COMPLEXES

Magnetic resonance imaging (MRI) is a noninvasive imaging technique that utilizes safe, nonionizing radiation for the diagnosis of early-stage diseases, including cancer. Although this technique provides a wealth of anatomical information, there are limitations in the information that MRI provides, such as the accurate local temperature in specific parts of the body. ^{51}V is a promising candidate for a high-resolution NMR thermometer due to its intrinsically low quadrupolar moment and subsequent narrow linewidth. Unlike other nuclei, such as ^{59}Co, design strategies for increasing the temperature sensitivity of ^{51}V complexes are currently unexplored. We present a route of amplifying temperature sensitivity of the ^{51}V chemical shift via ligand-to-metal charge transfer electronic structure design criteria. We demonstrate that this design strategy can boost the temperature dependence of the ^{51}V chemical shift by an order of magnitude.

TABLE OF CONTENTS

ACKNOWLEDGEMENTS

The author would like to acknowledge the members of both the Zadrozny group and the Crans group for all of their help and support during this project. Special thanks would like to be given to Joe Zadrozny and Debbie Crans for their support and mentorship. In addition to his mentors and lab mates, the author also wants to acknowledge Colorado State University for supporting this research.

DEDICATION

This thesis is dedicated to my friends and family who have supported me throughout my academic career as well as my newborn daughter, Adriana. Thank you all for everything you've all done!

LIST OF FIGURES

NMR Thermometry of Vanadium Based LMCT Complexes

1.1 Introduction

Designing molecules with variable-temperature magnetic resonance characteristics is vital to non-invasive imaging of temperature[1,2] – a key means of monitoring thermal procedures[3] and deeper understanding of physiological temperature management. One key feature, the nuclear magnetic resonance (NMR) chemical shift (d) is a particularly promising reporter for local temperature.[4] The nuclei of metal ions (e.g. ^{59}Co or ^{51}V) are particularly promising as d is strongly dependent on electronic structure and often span 1000s of ppm. In order to harness this advantage, we need to understand how to control the temperature sensitivity ($\Delta\delta/\Delta T$) by design.

Some of us have recently reported studies of controlling the temperature sensitivity of the ^{59}Co nuclear magnetic resonance chemical shift.[5-7] This nucleus generally exhibits a highly temperature-sensitive chemical shift (δ) in Co(III) complexes ($\Delta\delta/\Delta T$, > 2 ppm/°C) relative to other nuclei (e.g. ^{1}H, 0.01 ppm/°C or ^{19}F, 0.05 ppm/°C)[2,8] and is therefore promising for non-invasive imaging. In one case, we set a record for the temperature sensitivity of d for *all* nuclei, 150 ppm/°C, by exploiting the phenomenon of spin-crossover in a Co(III) complex.[5] In all these cobalt complexes, the spectroscopic linewidths are large (*ca*. 150 ppm), in part because of the quadrupolar moment, which accelerates spin relaxation for

the ^{59}Co nucleus.[9] A large linewidth is disadvantageous for imaging, because broadening lowers sensing resolution.

We propose ^{51}V as a potentially promising nucleus for high resolution NMR thermometry alternative to ^{59}Co, because ^{51}V possesses an intrinsically low quadrupolar moment.[10] However, design strategies for temperature sensitivity for the ^{51}V nucleus are currently unexplored (**Fig. 1**). We note that ^{51}V possesses no d electrons in the most common NMR-active oxidation state, V(V). Hence, the relevant energy gaps that direct a temperature dependent paramagnetic shift (via Ramsey's equation)[11] are not d-d excitations like for Co(III), and instead are likely ligand-to-metal charge transfer (LMCT) states. We hypothesized that explicit tuning of these states could provide the first design strategy for amplifying temperature sensitivity in ^{51}V NMR spectroscopy (**Fig. 1**). Importantly, we

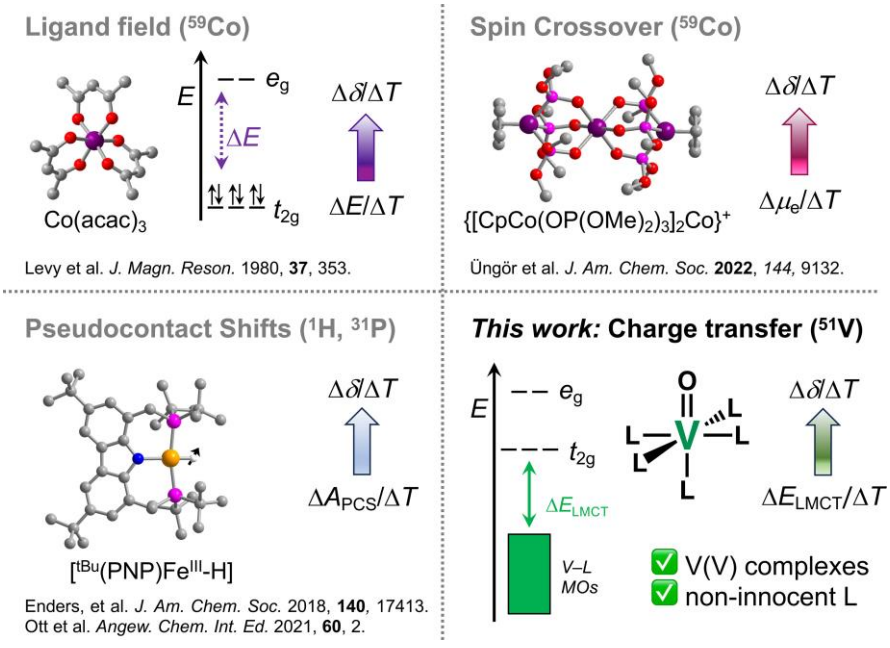

Fig. 1. Non-exhaustive graphical overview of different design strategies for temperature sensitivity in NMR chemical shifts with example molecules. The bottom right is the strategy tested in this paper.

hypothesized that noninnocent ligands would be desirable for this purpose, as they ensure high-energy frontier MOs for low-energy LMCTs.

To test the foregoing hypotheses, we herein report the structure, electronic spectroscopy, and variable-temperature ^{51}V NMR spectroscopic properties of a series of three complexes: [VO(EtHshed)(tbad)] (**1**, tbad = 5-(adamantan-1-yl)-3-(tert-butyl)benzene-1,2-diol, EtHshed = (*E*)-2-ethoxy-6-(((2-((2-hydroxyethyl)amino)ethyl)imino)methyl)phenol), [VO(EtHshed)(cat)] (**2**, cat = catechol), and [VO_2(EtHshed)] (**3**). In **1** and **2**, the presence of the tbad and catecholate ligands insert filled, high-energy ligand orbitals that support the existence of a low-energy LMCT, which is absent for **3**. Crucially, **1** and **2** also exhibit an order of magnitude higher $\Delta\delta/\Delta T$, *ca*. 0.6 to 0.7 ppm/°C, relative to **3** (0.07 ppm/°C). These data support the interpretation that LMCT considerations are one viable path toward amplifying $\Delta\delta/\Delta T$ for ^{51}V NMR thermometers.

1.2 Experimental

Syntheses of **1** and **2** is prepared from the pre-cursor Schiff base complex **3**. Complex **3** is prepared from the condensation reaction of 3-ethoxy salicylaldehyde and N-(2-hydroxyethyl) ethylenediamine followed by the addition of vanadyl sulfate in degassed methanol, as reported previously.[12] Syntheses of **1** and **2** proceed by addition of tbad and catechol, respectively, in degassed methanol to the yellow product , **3**, as reported previously for other noninnocent vanadium Schiff base complexes.[12] Upon the addition of either tbad or catechol to **3**, the colors of the reaction mixtures change from faint yellow to a deep, intense purple color.

1.3 Results

The geometry of **1** contains a distorted octahedral vanadium atom in the crystalline state which presumably also is present in both **2** and **3**. (**Fig. 2**) Note that **3** exists both as a monomer and dimer of two [VO_2(Hshed)] units[12] which likely disassociate in solution as dimers of this general class are known to do.[13,14]

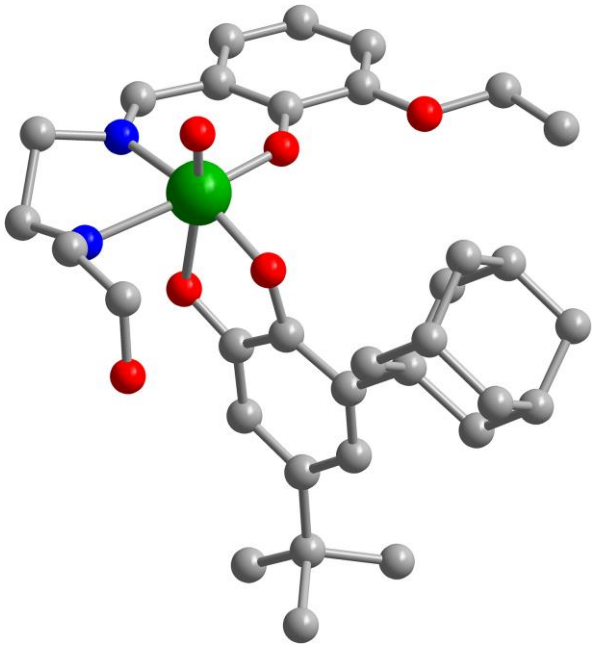

Fig. 2. Molecular structure of [VO(EtHshed)(tbad)] as present in the crystal structure of **1**. Green, red, blue, and gray spheres represent vanadium, oxygen, nitrogen, and carbon atoms, respectively. H atoms are omitted for clarity.

In **3**, the bond distance for the V-O bond is 1.616(3) Å, which is typical for a V(V) oxo group.[15] For **1,** the bond distance of the V-O bond is 1.591(7) Å, which is also in the expected range for V(V) oxo group. The C–O bond distances for catechol in **1** are 1.31(1) Å and 1.328(9) Å, which is shorter than the observed value of approximately 1.35 Å in free catechol.[16] This bond is however longer than the expected value of 1.29 Å in a reduced semiquinone radical[17] and much longer

than the expected value of 1.22 Å in a reduced *o*-benzoquinone.[18] These observations are consistent with all complexes being V(V) oxos bound to catecholate ligands.

In contrast to the yellow color of **3,** complexes **1** and **2** are dark purple and burgundy, respectively. The UV-Vis spectrum for **1** has three distinguishable peaks at 288 nm (6500 $M^{-1}cm^{-1}$), 551 nm (2063 $M^{-1}cm^{-1}$) and 862 nm (2375 $M^{-1}cm^{-1}$). (**Fig.3**) Complex **2** has four peaks at 223 nm (15374 $M^{-1}cm^{-1}$), 284 nm (7626 $M^{-1}cm^{-1}$), 531 nm (2200 $M^{-1}cm^{-1}$), and 865 nm (2956 $M^{-1}cm^{-1}$). (**Fig.3**) The magnitude of the extinction coefficient for the three lower energy peaks coupled with the fact that V(V) has 0 d-electrons suggests that these peaks are low energy LMCT bands for **1** and **2**.[19] In contrast, the UV-Vis spectrum for **3** shows three

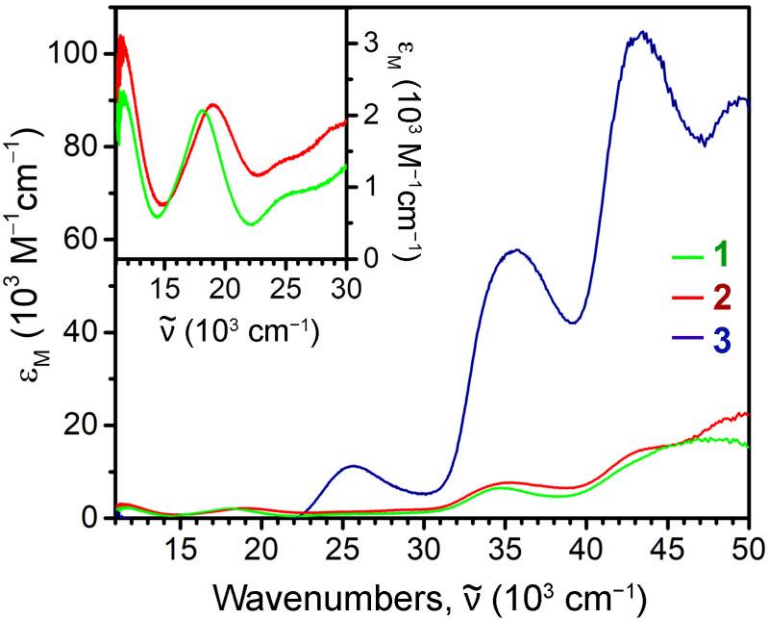

Fig. 3. UV-Vis spectra for **1**, **2**, and **3.** Inset: close up of low-energy charge transfer bands for **1** and **2**. Data were collected on solutions of **1-3** in CH_3CN with 0.1-0.3 mM concentrations.

distinguishable peaks at 230 nm (77667 $M^{-1}cm^{-1}$), 281 nm (42333 $M^{-1}cm^{-1}$), and 390 nm (8000 $M^{-1}cm^{-1}$). (**Fig.3**) The extinction coefficients for these peaks suggest that they could also be attributed to LMCT bands or LLCT bands. In either case, they are at a notably higher energy than the bands in **1** and **2**, and likely stem from the absence of a catecholate-like ligand.

The ^{51}V NMR spectra at ambient temperature for **1** and **2** are consistent with the presence of isomers in solution; the possibility that the signals are simple impurities was ruled out. The ^{51}V NMR spectra of **1** gives peaks for four isomers in solution, with three smaller peaks at 466 ppm (**1d**), 450 ppm (**1c**), 422 ppm (**1b**), and then the major peak at 373 ppm (**1a**). The asymmetry of the tbad ligand and potential hydrogen bonding in the coordination shell is likely contributing to the observation of these isomers.[20] For **2,** the ^{51}V NMR spectra gives two isomeric peaks in solution at 204 ppm (**2a**, the major peak) and 258 ppm (**2b**). In this species, the catecholate ligand is symmetric, and we see half as many isomers as **1**, suggesting ligand asymmetry contributes to the isomer distribution. In contrast to both **1** and **2**, the ^{51}V NMR spectra for **3** shows only one peak, at –525 ppm. The chemical shifts of **1**, **2**, and **3** follow expectations for V(V) species with (and without) noninnocent ligands.[21,22] Importantly, the ^{51}V δ values for **1-3** also trend with the observed energies of the LMCT transitions in the UV-Vis spectra: a lower energy LMCT accompanies a complex with a more downfield ^{51}V δ.

Next, we analyzed the variable-temperature ^{51}V NMR spectra of **1-3** in CH_3CN to determine how affected the $\Delta\delta/\Delta T$ of the ^{51}V NMR signals are in **1** and **2** relative

to the signals in **3**. Measurements were all made at ca. 105 MHz for ^{51}V over a 10 to 50 °C window with a 400 MHz (^{1}H) NMR magnet. For **1** and **2**, the temperature dependence of each isomer's peak can be clearly tracked, and all peaks shift downfield with increasing temperature. The major peak of **1** shows a $\Delta\delta/\Delta T$ of 0.60(1) ppm/ºC from 10-50ºC. The other minor peaks, in order of increasing δ, show temperature sensitivities of 0.70(1), 0.46(1), 0.77(1) ppm/ºC, respectively. (**Fig. 4a**) The peaks for **1** also broaden with increasing temperature, showing linewidth changes from 3 to 5 ppm over the measured window consistent with isomer interconversions. For **2,** ^{51}V δ of the major peak shifts by 0.67(1) ppm/ºC and the minor peak shifts by 0.74(1) ppm/ºC from 10-50 ºC. (**Fig. 4b**) Both isomers see a broadening in linewidth as the temperature increases from 3 ppm at 10ºC to 5 ppm at 50 ºC. In contrast, the ^{51}V chemical shift of **3** is virtually

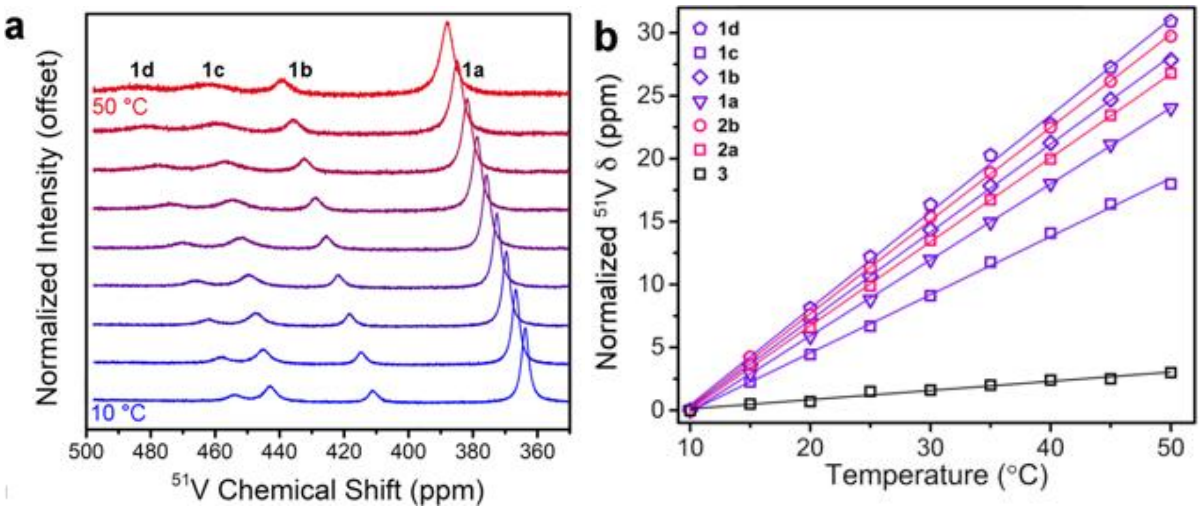

Fig. 4. **(a)** Variable-temperature ^{51}V NMR spectra for **1** collected with a 400 MHz (^{1}H) system and concentration of 10 mM in CH_3CN. The four observed peaks are different isomers of the complex and are labeled. **(b)** Relative chemical shift changes with temperature for **1**, **2**, and **3**, all normalized toward a 10 °C ^{51}V δ of 0 ppm. Solid lines are fits as a result of linear regression to give $\Delta\delta/\Delta T$ values described in the text.

temperature insensitive: the ^{51}V δ changes only by 0.07(1) ppm/ºC from 10-50 ºC with insignificant change in linewidth. (**Fig. 4b**)

1.4 Discussion

The observation of a high sensitivity for ^{51}V signals in **1** and **2**, but not in **3**, trends with the presence of a low-energy and the catecholate-type ligands. Hence, these results highlight the importance of the presence of the noninnocent ligand design strategies for ^{51}V NMR thermometers with a high $\Delta\delta/\Delta T$. These values are in the ballpark of high-temperature sensitivity of the ^{51}V species, e.g. $VO(Oi\text{-}pr)_3$ (0.61 ppm/ºC),[10] but lower than reported $(C_5H_5)V(CO)_3L$ complexes, which can exhibit temperature sensitivities close to 1.2 ppm/ºC.[23] The current record $\Delta\delta/\Delta T$ for a V(V) complex belongs to $[V(NO)_2(THF)_4]Br$ with a shift of 1.23 ppm/ºC, also higher than that observed for compound **1**.[24] These species all possess different low-valent oxidation states, V(I–) and V(I+), and feature organometallic or other reactive ligand shells that are disadvantageous for bioimaging applications relative to **1-3**. Compounds **1** and **2** hold the record temperature sensitivities for V(V) complexes, and their ligand shells are compatible with biological applications.[18,23]

A final point worth considering in these molecules concerns the ^{51}V NMR linewidths. A linewidth, $\nu_{1/2}$, of 3-5 ppm, as we found over the entire range of measurement of **1-3**, is in general smaller than the typical linewidths for competitor ^{59}Co thermometer systems, which can have 10s to 100s of ppm linewidths. The ratio of the temperature sensitivity to the linewidth $(\Delta\delta/\Delta T)/\nu_{1/2}$

yields the resolution of the thermometry. For **1-3**, these resolutions are *ca*. 0.1-0.24 °C^{-1} for **1**, 0.26-0.33 °C^{-1} for **2**, and 0.03 °C^{-1} for **3**. These values are smaller than the ^{59}Co-based temperature-sensitive systems, e.g. 3.66 °C^{-1} for Co(acac)$_3$ and 1.18 °C^{-1} for [(CpCo(OP(O*t*Bu)$_2$)$_3$)$_2$]Co$^+$, though close to the 0.28 °C^{-1} for [*t*Bu(PNP)Fe–H] (which exhibit 10-30 ppm/°C $\Delta\delta/\Delta T$ for ^{1}H and ^{31}P). [5,25-276] These observations highlight the need for further optimization studies.

The ability to design higher temperature sensitivities from magnetic resonance responses is vital toward design of novel non-invasive thermometers. The foregoing data reveal the first design strategy for amplifying temperature sensitivity for ^{51}V NMR signals in V(V) complexes, namely, the inclusion of LMCT bands. LMCT bands are tied to the complex's structures, their ability to penetrate cells, and their signals are readily tunable for the application of potential probes. We anticipate a valuable body of information on tuning $\Delta\delta/\Delta T$ to stem from investigating how structural changes impact ^{51}V temperature-dependent properties will identify a number of potential temperature probes. Ligand-tuning studies of this type are ongoing and will be reported in due course.

References

(1) Winter, L.; Oberacker, E.; Paul, K.; Ji, Y.; Oezerdem, C.; Ghadjar, P.; Thieme, A.; Budach, V.; Wust, P.; Niendorf, T. "Magnetic resonance thermometry: Methodology, pitfalls and practical solutions" *Int. J. Hypertherm.* **2016**, *32* (1), 63-75.

(2) Rieke, V.; Pauly, K. B. "MR thermometry" *J. Magn. Reson. Imaging* **2008**, *27* (2), 376-390.

(3) van Rhoon, G. C.; Wust, P. "Introduction: Non-invasive thermometry for thermotherapy" *Int. J. Hypertherm.* **2005**, *21* (6), 489-495.

(4) Brateman, L. "Chemical shift imaging: a review" *Am. J. Roentgenol.* **1986**, *146* (5), 971-980.

(5) Üngör, Ö.; Ozvat, T. M.; Ni, Z.; Zadrozny, J. M. "Record Chemical-Shift Temperature Sensitivity in a Series of Trinuclear Cobalt Complexes" *J. Am. Chem. Soc.* **2022**.

(6) Ozvat, T. M.; Rappé, A. K.; Zadrozny, J. M. "Isotopomeric Elucidation of the Mechanism of Temperature Sensitivity in ^{59}Co NMR Molecular Thermometers" *Inorg. Chem.* **2022**, *61* (2), 778-785.

(7) Ozvat, T. M.; Peña, M. E.; Zadrozny, J. M. "Influence of ligand encapsulation on cobalt-59 chemical-shift thermometry" *Chem. Sci.* **2019**, *10* (27), 6727-6734.

(8) Berkowitz, B. A.; Handa, J. T.; Wilson, C. A. "Perfluorocarbon temperature measurements using 19F NMR" *NMR in Biomedicine* **1992**, *5* (2), 65-68.

(9) Chan, J. C. C.; Au-Yeung, S. C. F. "Cobalt-59 NMR spectroscopy" *Annu. Rep. NMR Spectrosc.* **2000**, *41*, 1-54.

(10) Rehder, D.; Polenova, T.; Bühl, M. "Vanadium-51 NMR" *Annu. Rep. NMR Spectrosc.* **2007**, *62*, 49-114.

(11) Ramsey, N. F. "Magnetic Shielding of Nuclei in Molecules" *Phys. Rev.* **1950**, *78* (6), 699-703.

(12) Wang, F.-M. "Di-[mu]-oxido-bis[(2-ethoxy-6-{[2-(2-hydroxyethylamino)ethylimino]methyl}phenolato-[kappa]3N,N',O1)oxidovanadium(V)]" *Acta Crystallographica Section E* **2012**, *68* (1), m26-m27.

(13) Kober, E.; Nerkowski, T.; Janas, Z.; Jerzykiewicz, L. B. "Vanadate complexes bearing an imidazolidine-bridged bis(aryloxido) ligand: synthesis and solid state and solution structure" *Dalton Trans.* **2012**, *41* (17), 5188-5192.

(14) Maurya, M. R. "Probing the synthetic protocols and coordination chemistry of oxido-, dioxido-, oxidoperoxido-vanadium and related complexes of higher nuclearity" *Coord. Chem. Rev.* **2019**, *383*, 43-81.

(15) Schindler, M.; Hawthorne, F. C.; Baur, W. H. "Crystal Chemical Aspects of Vanadium: Polyhedral Geometries, Characteristic Bond Valences, and Polymerization of (VOn) Polyhedra" *Chem. Mater.* **2000**, *12* (5), 1248-1259.
(16) Brown, C. "The crystal structure of catechol" *Acta Crystallographica* **1966**, *21* (1), 170-174.
(17) Adams, D. M.; Dei, A.; Rheingold, A. L.; Hendrickson, D. N. "Bistability in the [CoII(semiquinonate)2] to [CoIII(catecholate)(semiquinonate)] valence-tautomeric conversion" *J. Am. Chem. Soc.* **1993**, *115* (18), 8221-8229.
(18) Macdonald, A. L.; Trotter, J. "Crystal and molecular structure of o-benzoquinone" *J. Chem. Soc., Perkin trans. 2* **1973**, (4), 476-480.
(19) Holmes, S.; Carrano, C. J. "Models for the binding site in bromoperoxidase: mononuclear vanadium(V) phenolate complexes of the hydridotris(3,5-dimethylpyrazolyl)borate ligand" *Inorg. Chem.* **1991**, *30* (6), 1231-1235.
(20) Murakami, H. A.; Uslan, C.; Haase, A. A.; Koehn, J. T.; Vieira, A. P.; Gaebler, D. J.; Hagan, J.; Beuning, C. N.; Proschogo, N.; Levina, A.; Lay, P. A.; Crans, D. C. "Vanadium Chloro-Substituted Schiff Base Catecholate Complexes are Reducible, Lipophilic, Water Stable, and Have Anticancer Activities" *Inorg. Chem.* **2022**, *61* (51), 20757-20773.
(21) Goncharova-Zapata, O.; Chatterjee, P. B.; Hou, G.; Quinn, L. L.; Li, M.; Yehl, J.; Crans, D. C.; Polenova, T. "Effect of ancillary ligand on electronic structure as probed by 51V solid-state NMR spectroscopy for vanadium–o-dioxolene complexes" *CrystEngComm* **2013**, *15* (43), 8776-8783.
(22) Chatterjee, P. B.; Goncharov-Zapata, O.; Quinn, L. L.; Hou, G.; Hamaed, H.; Schurko, R. W.; Polenova, T.; Crans, D. C. "Characterization of Noninnocent Metal Complexes Using Solid-State NMR Spectroscopy: o-Dioxolene Vanadium Complexes" *Inorg. Chem.* **2011**, *50* (20), 9794-9803.
(23) Jameson, C. J.; Rehder, D.; Hoch, M. "Isotope and temperature dependence of transition-metal shielding in complexes of the type M(XY)6" *J. Am. Chem. Soc.* **1987**, *109* (9), 2589-2594.
(24) Näumann, F.; Rehder, D.; Pank, V. "Transition metal nitrosyls as nitrosylation agents. IV. 51V NMR characteristics of dinitrosyl and carbonylmononitrosyl vanadium complexes" *Inorg. Chim. Acta* **1984**, *84* (1), 117-123.
(25) Levy, G. C.; Bailey, T. J.; Wright, D. A. "A sensitive NMR thermometer for multinuclei FT NMR" *J. Magn. Reson.* **1980**, *37* (2), 353-356.
(26) Ott, J. C.; Wadepohl, H.; Enders, M.; Gade, L. H. "Taking Solution Proton NMR to Its Extreme: Prediction and Detection of a Hydride Resonance in an Intermediate-Spin Iron Complex" *J. Am. Chem. Soc.* **2018**, *140* (50), 17413-17417.
(27) Ott, J. C.; Suturina, E. A.; Kuprov, I.; Nehrkorn, J.; Schnegg, A.; Enders, M.; Gade, L. H. "Observability of Paramagnetic NMR Signals at over 10 000 ppm Chemical Shifts" *Angew. Chem. Int. Ed.* **2021**, *60* (42), 22856-22864.

Appendix A-Supplementary Information

General Considerations. Reagents used throughout were purchased from commercial sources and used as received. All techniques were performed at atmospheric conditions unless otherwise specified. Solvents were purchased and used as received.

Synthesis of VO2(EtHshed) (3). Synthesis of this compound followed a modified procedure of a literature preparation.1 To a 100 ml Schlenk flask, 40 ml of HPLC- grade methanol was added and degassed with argon for 7 minutes. This was followed by the addition of 3-ethoxy-salicylaldehyde (1.562 g, 9.400 mmol) and N-(2-hydroxyethyl) ethylenediamine (0.979 g, 9.40 mmol). The reaction mixture was let to stir for an hour at ambient temperature under argon. Vanadyl sulfate (1.866 g, 11.45 mmol), dissolved in 25 ml degassed water, was added to the reaction mixture after 1 hour. The reaction mixture was let then to stir for 3 hours at ambient temperature under argon. After 3 hours, sodium hydroxide (0.752 g, 18.8 mmol) was added, the reaction mixture was opened to air and let to stir overnight. The product then was vacuum filtered, washed with 25 ml cold (0 □C) methanol and left to dry under high vacuum for 3 days. Yield 58%. δ 1H NMR (400 MHz, CDCl3) δ 8.74 ppm (s, 1H) 7.11 ppm (m, 2H) 6.80 (t, 1H) 4.30 (m, 2H) 3.90 (m, 2H) 3.36 (m, 2H) 3.05 (m, 2H) 2.76 (m, 2H) 1.42 (t, 3H).

Synthesis of VO(Hshed)(tbad) (1). To a clean, dry 100 mL Schlenk flask, 25 mL of HPLC-grade methanol was added and degassed with nitrogen for 15 minutes. Following this, VO2(EtHshed) (0.334 g, 1.000 mmol) was added to the methanol followed by 3-(tert-

butyl)-5-(adamant-1-yl) catechol (0.379 g, 1.000 mmol). Immediately after the addition of the catechol, the reaction mixture was placed under nitrogen. Upon the addition of the catechol, the color slowly changed from yellow to brown to dark violet. The reaction mixture was allowed to stir overnight under nitrogen. The solution was then filtered in vacuo and the filtrate was then evaporated to complete dryness via rotary evaporator. To the resulting solid was then dissolved in minimal GC-Resolv grade acetone followed by the addition of ACS-grade hexanes (100 mL). The solution was then capped and stored at –20 ºC overnight to precipitate out the desired purple solid. X-ray quality crystals were grown by minimally dissolving the powder into acetone and layering with hexanes followed by storing at –20 ºC for two weeks until crystals appeared. Yield: 41%. δ51V NMR (101 MHz, CD3CN) δ 372 ppm (major) 422 ppm (minor) 450 ppm (minor) 466 ppm (minor). δ 1H NMR (400 MHz, CDCl3) δ 8.33 ppm (s, 1H) 7.01 ppm (d, 1H) 6.94 ppm (d, 1H) 6.60 ppm (t, 1H) 6.34 ppm (s, 1H) 6.22 ppm (s, 1H) 3.98 ppm (m, 4H) 3.88 ppm (m, 2H) 3.63 ppm (m, 1H) 3.44 ppm (m, 1H) 3.32 ppm (m, 1H) 3.14 (m, 1H) 2.09 ppm (s, 6H) 1.81 (m, 8H) 1.58 ppm (s, 3H) 1.21 ppm (s, 9H) 0.86 ppm (t, 3H). Combustion analyses calculated for H45C33N2O6V (found) 64.27 (62.80) % C; 7.36 (7.36) % H; 4.54 (4.42) % N.

Synthesis of VO(EtHshed)(cat) (2). To a clean, dry 100 mL Schlenk flask, 25 mL of HPLC-grade methanol was added and degassed with nitrogen for 15 minutes. Following this, VO2(EtHshed) (0.167 g, 0.500 mmol) was added to the methanol followed by catechol (0.055 g, 0.500 mmol). Immediately after the addition of the catechol, the reaction mixture was placed under nitrogen. Upon the addition of the catechol, the color

slowly changed from yellow to brown to dark violet. The reaction mixture was allowed to stir overnight under nitrogen. The solution was then filtered in vacuo and the filtrate was then evaporated to complete dryness via rotary evaporator. To the resulting solid was then dissolved in minimal GC-Resolv grade acetone followed by the addition of ACS-grade hexanes (100 mL). The solution was then capped and stored at -20 ºC overnight to precipitate out the desired purple solid. Yield: 66%. δ51V NMR(101 MHz, CD3CN) δ 204 ppm (major) 259 ppm (minor). δ 1H NMR (400 MHz, CDCl3) δ 8.42 ppm (s, 1H) 7.14 ppm (d, 1H) 7.07 ppm (d, 1H) 7.01 ppm (d, 1H) 6.70 ppm (t, 1H) 6.58 ppm (d, 1H) 6.47 ppm (d, 1H) 6.38 ppm (d, 1H) 4.21 ppm (m, 1H) 4.02 ppm (m, 4H) 3.86 ppm (m ,1H) 3.68 ppm (m, 1H) 3.50 ppm (m, 1H) 3.34 ppm(m, 1H) 3.07 ppm (m, 1H) 1.66, (s, 2H) 1.23 ppm (t, 3H). Combustion analyses calculated for H23C36N2O6V (found) 53.53 (53.36) % C; 5.44 (5.45) % H; 6.57 (6.32) % N.

^{51}V NMR Analyses. Solution-phase ^{51}V NMR analyses were performed with an Agilent (Varian) 400 NMR equipped with Automated Tuning and a 7620 96-slot Sample Changer. At the field of this instrument, the ^{51}V NMR signal is ca. 104.5 MHz. All samples were prepared at ca. 50 mM concentrations under air in the indicated solvents.

X-ray Data Collection, Structure Solution and Refinement for 1. Diffraction data were collected at the X-Ray Diffraction facility of the Analytical Resources Core at Colorado State University. Data were collected on a Bruker D8 Quest ECO single-crystal X-ray diffractometer equipped with Mo Kα (λ = 0.71073 Å). Data were collected and integrated using Bruker Apex 3 software. Absorption corrections were applied using SADABS.3 Space group assignments were determined by examination of systematic absences, E-

statistics, and successive refinement of the structures. Crystal structures were solved using SHELXT and refined with the aid of successive difference Fourier maps by SHELXL operated in conjunction with OLEX2 software.4–6 None of the crystals demonstrated decay by X-ray radiation over the course of the experiment. Hydrogen atoms were placed in ideal positions and refined using a riding model for all structures.

Other Physical Measurements. Elemental analyses were performed by Roberson Microlit Laboratories (Ledgewood, New Jersey, USA). UV-Vis spectra were collected by using a Shimadzu UV-2600i UV-Vis spectrophotometer, using standard quartz cuvettes with a 1 cm path length with CH_3CN solvent. Proton (^1H) NMR analyses were performed on a Bruker ASCEND 400 MHz NMR with BBFO smart probe.

Appendix Table 1. Crystallographic information for the structural refinement of **1**.

Empirical formula	$H_{51}C_{36}N_2O_7V$
Formula Weight	674.75 g/mol
Temperature	100(2)
Crystal System	Orthorhombic
Space Group	$P2_12_12_1$
a	12.4459(6) Å
b	12.6480(6) Å
c	21.7984(10) Å
α	90°
β	90°
γ	90°
Volume	3431.41(30) $Å^3$
Z	4
ρ_{calc}	1.30603 g/cm^3
μ	0.340 mm^{-1}
F(000)	1440
Crystal Color	Violet
Crystal Size	0.262 x 0.093 x 0.064 mm^3
Radiation	MoKα (λ=0.71073 Å)
2θ range for data collection	1.868 to 24.108°
Index ranges	$-14 \leq h \leq 14$, $-14 \leq k \leq 14$, $-25 \leq l \leq 25$
Reflections collected	63283
Independent Collections	5449 [R_{int}=0.0687, R_{sigma}=0.0292]
Data/restraints/parameters	5449/3/441
Goodness-of-fit on F^2	1.17
Final R indexes ($I \geq 2\sigma$ (I)]	R_1 = 0.0688, wR_2=0.1574
Final R indexes [all data]	R_1=0.0788, wR_2=0.1501
Largest diff. peak/hole	0.742/-0.590 e $Å^{-3}$

Appendix Figure 1. 1H NMR Spectra for **3**.

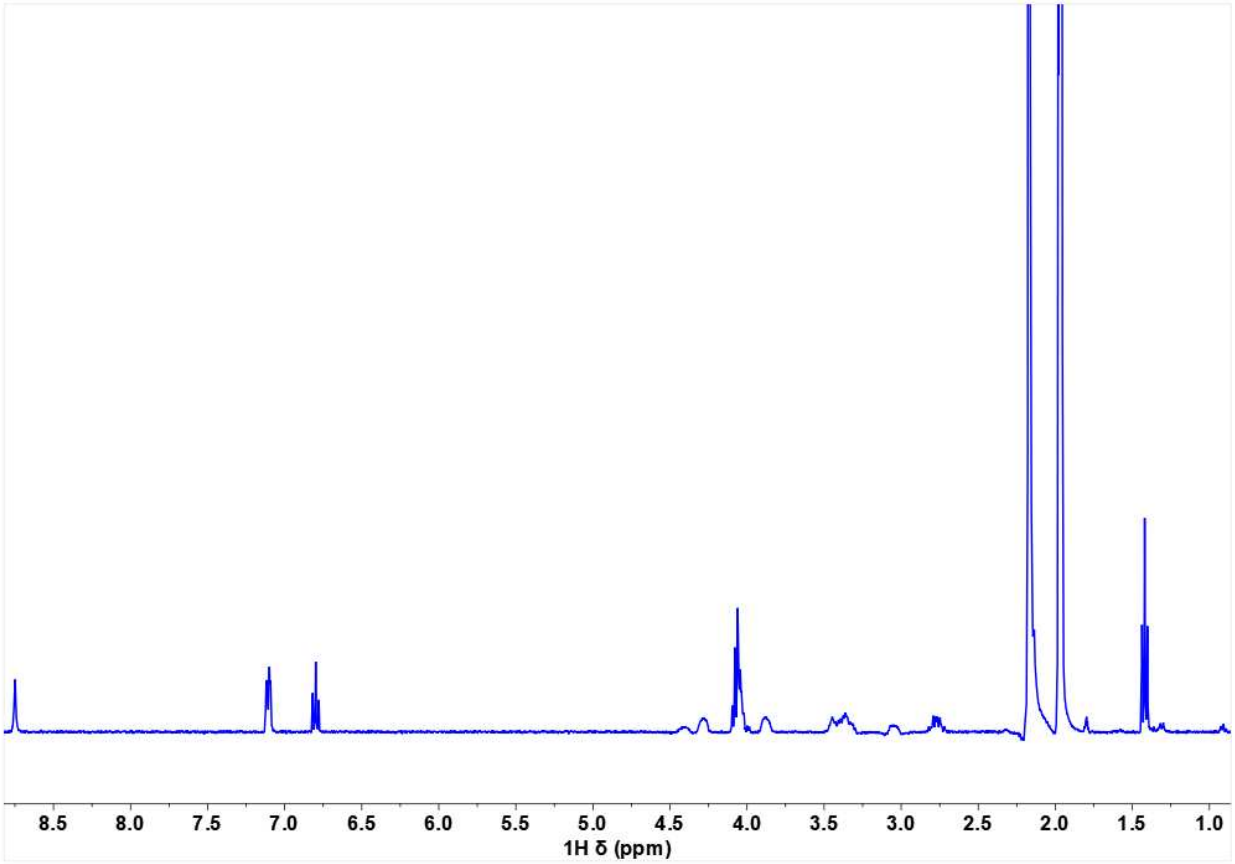

Appendix Figure 2. Variable Temperature ^{51}V NMR Spectra for **3**.

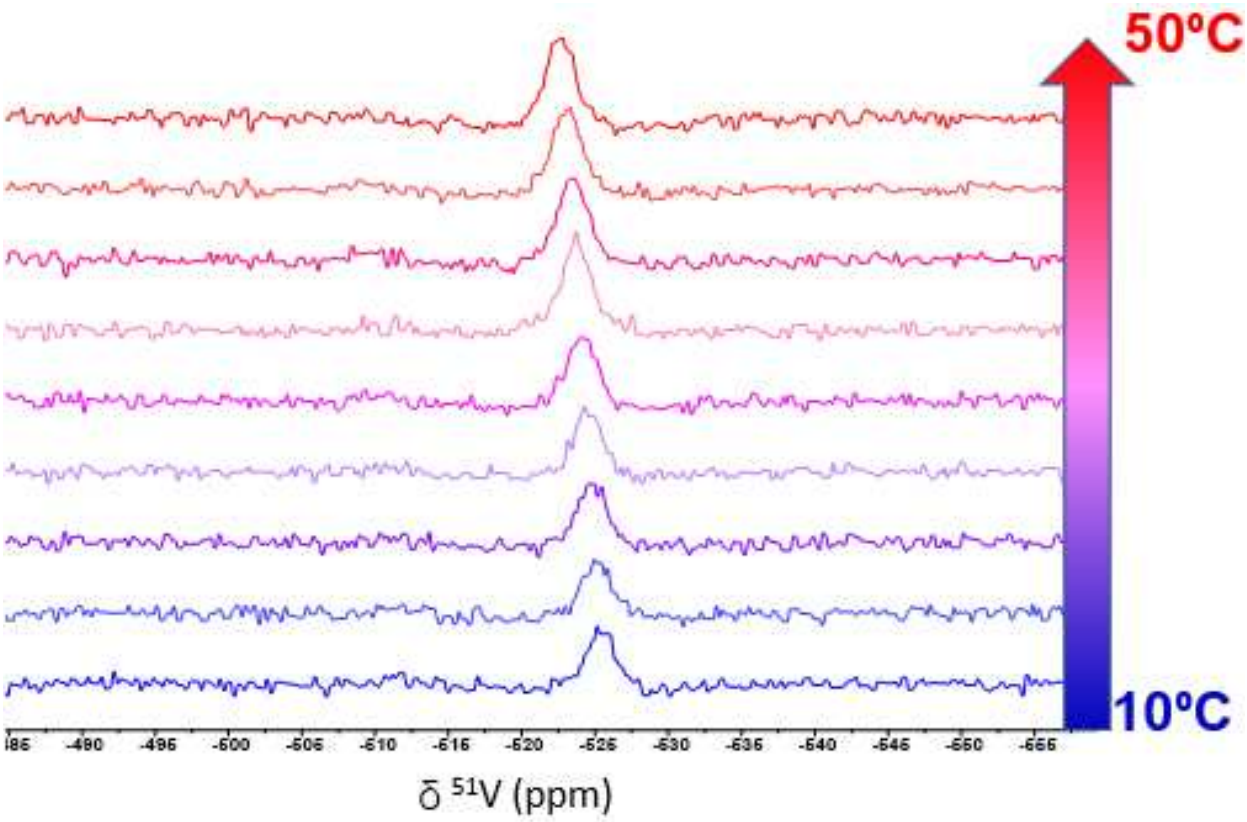

Appendix Figure 3. Variable Temperature ^{51}V NMR Spectra for **2**.